

Calculation of linear/non-linear optical response functions of large quantum systems by real-time real-space higher-order finite-difference method

Yoshiyuki Kurokawa,^{*1,*2} Shintaro Nomura,^{*3} Tadashi Takemori,^{*1} and Yoshinobu Aoyagi^{*2}

^{*1} *Institute of Materials Science, University of Tsukuba*

^{*2} *Semiconductors Laboratory, RIKEN*

^{*3} *Institute of Physics, University of Tsukuba*

We report the state of progress in the application of the real-time real-space higher-order finite-difference method which is effective in computing electronic properties of large quantum systems. With the use of empirical pseudopotentials, the effectiveness of the method has been demonstrated in the calculation of absorption spectra of such realistic systems as hydrogenated silicon nanocrystallites, silicon nanocrystals embedded in amorphous silicon, and polysilane. The method has proved also effective in calculating nonlinear response functions when used in conjunction with a newly developed fast algorithm.

Introduction

Every experimental measurement of a property of a material needs to be interpreted in terms of the underlying physics, and comparison with theoretical calculation provides a basic tool for such analysis. While a fully quantum-mechanical calculation has long been done for small molecules and crystals, a realistic calculation has been difficult for aperiodic systems and large molecules because of the sheer amount of computation involved. Examples of such systems include amorphous materials and systems with surfaces and interfaces. Calculation of quantum size effects in nanocrystallites poses a particular challenge in the light of the abundance of experimental data that are emerging lately in the literature.

The real-time real-space higher-order finite-difference method¹⁾ was developed in order to meet such challenges of computing electronic properties of complex systems on a fully quantum mechanical basis. In this method, the three-dimensional physical space is represented by discrete mesh points, and the time development of a system is solved by numerically integrating the Schrödinger equation for discrete time steps. Response functions can be obtained by directly simulating the time development under the influence of the external perturbation. This has the advantage of not requiring the knowledge of the energy eigenstates and eigenfunctions. If necessary, such knowledge can be obtained by Fourier-analyzing the numerical solution of the time development.

The formulation is not only straightforward to code, but is also particularly suitable for parallelization because all the operations involved are local in space-time. The method is an $O(N)$ method where both the memory requirement and the CPU time scale only linearly with the number of basis states N , compared to N^2 and N^3 , respectively, for matrix diagonalization.

The effectiveness of the method was first demonstrated in the calculation of the optical absorption spectra of hydro-

genated silicon nanocrystallites containing more than 10000 atoms.²⁾ It was then applied to silicon nanocrystals embedded in amorphous silicon.³⁾ Recently, we used the method to calculate the absorption spectra of aperiodic polysilane chains.⁴⁾ Besides applying the method to different materials, we recently developed a fast algorithm for calculating the nonlinear response functions,⁵⁾ and tested it on the two-photon absorption spectrum of crystalline silicon.⁶⁾ In this paper, we review such progress that we have been making during recent years in the application of the real-time real-space higher-order finite-difference method.

Linear response function and density of states

In the real-time real-space higher-order finite-difference method, the electronic density of states $\rho(\omega)$ and the dielectric function $\epsilon(\omega)$ are calculated according to the expressions;¹⁾

$$\rho(\omega) = -\frac{1}{\pi} \mathbf{Im} \left\langle \frac{1}{i\hbar} \int_0^T dt e^{i(\omega+i\eta)t} \langle \Phi | e^{-iHt} | \Phi \rangle \right\rangle_{\Phi} \quad (1)$$

and

$$\epsilon_{\beta\alpha}(\omega) = 1 + 4\pi \left\langle \int_0^T dt e^{-\eta t} (e^{i\omega t} - \delta_{\beta\alpha}) K_{\beta\alpha}(t) \right\rangle_{\Phi}, \quad (2)$$

where

$$K_{\beta\alpha}(t) = \frac{-2}{V(\omega+i\eta)} \mathbf{Im} \left\langle \Phi | \theta(E_F - H) e^{iHt} \times \mathbf{p}_{\beta} e^{-iHt} \theta(E_{cut} - H) \theta(H - E_F) \mathbf{p}_{\alpha} | \Phi \right\rangle. \quad (3)$$

Here $\alpha, \beta = x, y, z$, and $H, V, T, \theta(H), \mathbf{p}_{\alpha}, E_F$, and η are the Hamiltonian of the system, the volume of the system, the total time of integration, an operator step function, the electron momentum operator, the Fermi energy, and the energy resolution, respectively. The Hamiltonian is approximated by the discretized form in the real space according to the higher-order finite-difference method. The operator step function⁷⁾ $\theta(X)$ can be explicitly constructed for any

bounded Hermitian operator X without solving for the eigenvalues and eigenvectors. In our calculation, we use an algorithm based on Chebyshev polynomial expansion,⁷ which yields $\theta(X)$ as a polynomial of the operator X . The insertion of $\theta(E_{cut} - H)$ is made to reduce the statistical fluctuation in the calculated spectra originating from the unphysical high-energy components. The statistical averaging indicated by $\langle \dots \rangle_{\Phi}$ in Eqs. (1) to (3) is over the random realizations of the random phase vector⁸) $|\Phi\rangle = \sum_{n=1}^N |n\rangle e^{i\phi_n}$ where $|n\rangle$ are the basis vectors and $\phi_n (n = 1, \dots, N)$ are uniform random variables in the range $[-\pi, \pi)$. It can be shown that the averaging procedure is equivalent to calculating the trace of an operator,¹) and that the computation cost is $O(N)$. Since the random vector samples the Hilbert space randomly, it may be regarded as a variant of quantum Monte Carlo methods. A unique property of this method is that the statistical fluctuation is reduced not only by collecting a large number of random samples, but very effectively by increasing the dimension of the random vector.¹) This method is therefore particularly suitable for the calculation of large systems.

Quantum confinement effect in a hydrogenated Si nanocrystallite²)

Before proceeding to discuss a quantum size effect in nanocrystalline phase/amorphous phase Si structures, the quantum confinement effect in a hydrogenated Si nanocrystallite is briefly described. Higher energy shift of energy levels with reduction of the size of semiconductor quantum dots by gaining the kinetic energy due to spatial confinement of the electrons by a potential barrier is often referred to as a quantum confinement effect.^{9,10}) Hydrogen atoms on the surface surrounded by vacuum region create a confining potential barrier which is equivalent to the ionization energy of a hydrogenated Si nanocrystallite. The transition energy between the highest valence-hole state and the lowest conduction electron state (E_g) was calculated by tight-binding methods,¹¹) an LCAO-LDA method,¹²) an empirical pseu-

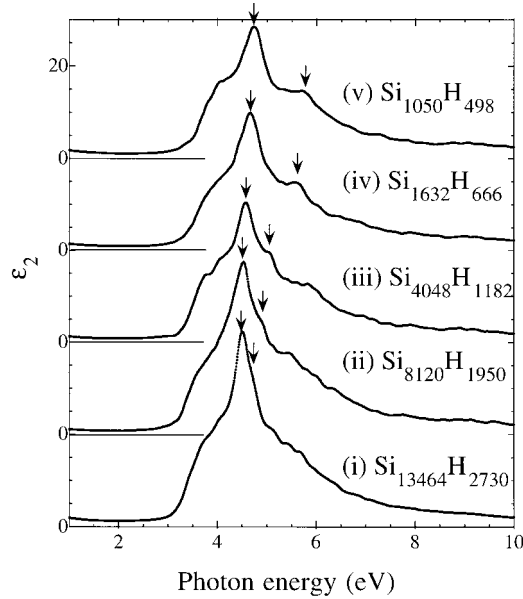


Fig. 1. Imaginary part of the dielectric function of hydrogenated Si (i) $\text{Si}_{13464}\text{H}_{2730}$, (ii) $\text{Si}_{8120}\text{H}_{1950}$, (iii) $\text{Si}_{4048}\text{H}_{1182}$, (iv) $\text{Si}_{1632}\text{H}_{666}$, and (v) $\text{Si}_{1050}\text{H}_{498}$. Zero points of the y axis are shifted as shown by the horizontal lines. The first peak and the second peak or shoulder are denoted by the arrows.

dopotentia method,¹³) and an *ab initio* real space calculation of the quasi particle band-gap.¹⁴) E_g was found to be proportional to $d^{-1.37}$ for the effective size of nanocrystallites d smaller than 3.41 nm.¹³) The peak energy of the absorption spectrum or the imaginary part of the dielectric function shows similar size dependence as E_g .^{2,15}) The imaginary part of the dielectric function ε_2 is shown in Fig. 1, calculated for cubic hydrogenated Si nanocrystallites with faces (110), $(1\bar{1}0)$, and (001). An empirical scaling law of $L_c^{-1.9}$ was deduced from fitting the peak energies of the calculated absorption spectra, where L_c is the length of the side of the cube of silicon atoms.²) The L_c dependence of the peak position of ε_2 will be used as a “reference” to discuss the quantum size effect in nanocrystalline phase/amorphous phase Si structures in what follows.

Quantum size effect in nanocrystalline/amorphous phase Si structures³)

To model a nanocrystalline phase/amorphous phase Si structure, we assume cubic supercells consisting of nanocrystalline phase and amorphous phase regions with (100) interface.¹⁶) The dimension of the supercell L is set to be integer multiples of the bulk lattice constant a_0 . A nanocrystalline phase region is defined by a cubic region L_c^3 , where L_c is also integer multiples of a_0 . An amorphous phase region fills in the region between the cubic regions L^3 and L_c^3 . In what follows, L and L_c in units of a_0 are used to denote the structures. For example, $\{8, 12\}$ denotes a structure with $L_c = 8a_0$ and $L = 12a_0$. A Monte Carlo method with the Metropolis algorithm for optimization of the atomic positions is applied to construct the model structures, which can be found in the literature.¹⁶) The order N method is used to calculate the complex dielectric function¹) of the model nanocrystalline phase/amorphous phase Si structures. In the constant L case, L_c is varied by keeping the total number of Si atoms

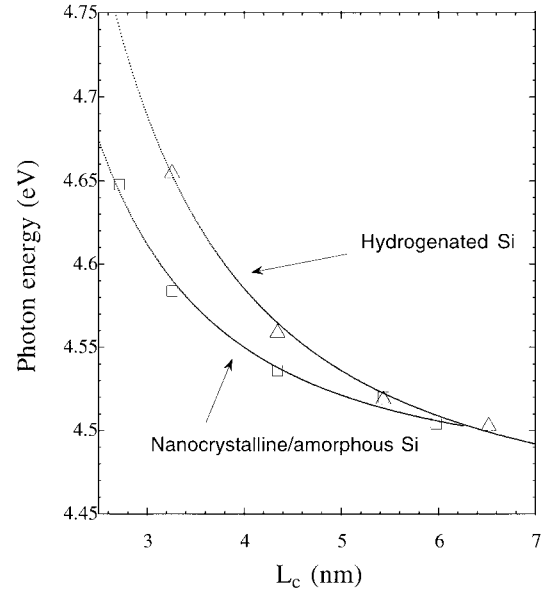


Fig. 2. L_c dependence of peak positions in ε_2 of nanocrystalline phase/amorphous phase Si inside the nanocrystalline region for models with L fixed to $12a_0$ (\square). A best fitted curve following an empirical scaling law of L_c^{-2} is shown. Size dependence of peak positions in ε_2 of hydrogenated Si nanocrystallites is also shown (\triangle) with a best fitted curve following $L_c^{-1.9}$.

fixed. The peak position of ε_2 shifts to higher energy with the decrease in L_c , which is clearly seen in Fig. 2. Both the decrease in L_c and the increase in the thickness of the amorphous phase region $L - L_c$ contribute to the higher energy shift of the peak position of ε_2 . The peak position of ε_2 is best fitted with a scaling law of L_c^{-2} as shown in Fig. 2. Our result indicates that the higher energy shift of the absorption spectra in the nanocrystalline/amorphous Si films with the decrease in size of the nanocrystalline region is due to a quantum size effect.³⁾ This is a novel quantum size effect without confinement of an electron, in contrast to the conventional usage of the “quantum size effect” synonymous with the “quantum confinement effect”.

Polysilane⁴⁾

Polysilane has recently attracted attention because of its peculiar optical properties.¹⁷⁾ It is a 1-dimensional chain $(\text{SiH}_2)_n$ connected by the tetrahedral bonds of Si atoms. The chain is known to take various conformations such as *trans* and *helix*, so that an actual polysilane chain must contain sections of different conformations. Then there must also be optical properties that are associated with section boundaries. Theoretical calculation, on the other hand, has only been done for periodic structures without boundaries.¹⁸⁾ We made use of the ample capability of the real-time real-space higher-order finite-difference method to calculate the electronic states and the optical properties of long aperiodic chains of polysilane. The absorption spectra of *helix*-polysilane chains are shown in Fig. 3. Pseudopotentials of silicon and hydrogen atoms are the same as those used in the calculation of silicon nanocrystallites.^{2,13)} The *helix*-polysilane chain is 40 nm long and contains 300 Si atoms. The curve (i) is for the periodic chain with no reversal of helicity. The curves (ii) and (iii) are for chains that have 2 and 4 section boundaries, respectively, where the helicity goes into reverse. A prominent difference between the three curves is the structure between 5.5 eV and 6 eV. The absence of peaks in this range for the periodic case suggests that the structure has its origin in the electronic states near the section boundaries. It is interesting that the number of peaks is 2 and 4 for the

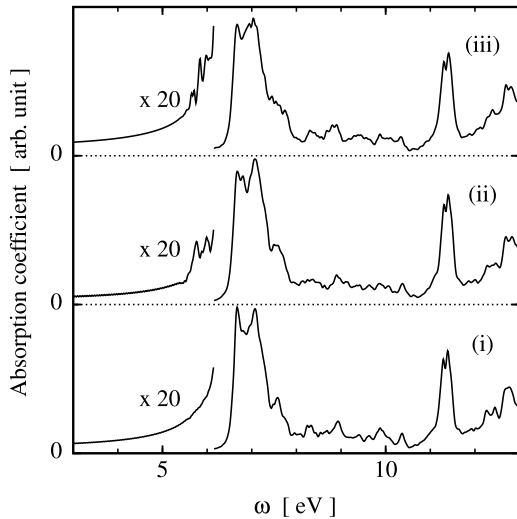


Fig. 3. The absorption spectra of *helix*-polysilane with different numbers of section boundaries.

curves (ii) and (iii), respectively. The fact that the number of peaks coincides with the number of section boundaries further lends support to the idea that the peaks are associated with electronic states that are localized at the boundaries. The calculation can be made to yield more direct information on the electronic wave function, and closer examination should give a definite clue as to the nature of these peaks.

Non-linear response function⁵⁾

Calculation of a non-linear response function of order n generally involves evaluating an n -dimensional integral of the form

$$\int_0^T dt_1 \int_0^{t_1} dt_2 \cdots \int_0^{t_{n-1}} dt_n e^{i(\omega_1 t_1 + \omega_2 t_2 + \cdots + \omega_n t_n)} \left\langle \langle \Phi | \hat{O}_f e^{iHt_1/\hbar} \hat{O}_1 e^{-iH(t_1-t_2)/\hbar} \hat{O}_2 e^{-iH(t_2-t_3)/\hbar} \cdots e^{-iH(t_{n-1}-t_n)/\hbar} \hat{O}_n e^{-iHt_n/\hbar} \hat{O}_i | \Phi \rangle \right\rangle_{\Phi}. \quad (4)$$

If Eq. (4) were to be numerically implemented straightforwardly, the matrix element inside the integral would have to be evaluated for all possible combinations of the time variable t_i 's. One would then start with a random vector $|\Phi\rangle$, solve the time development according to the Schrödinger equation, multiplying operators (\hat{O} 's) along the way as required, and take the inner product with $\langle \Phi |$ at the end. The number of discrete time steps required for a calculation of energy resolution η scales as η^{-1} , so that the direct implementation of Eq. (4) requires a computation load that grows as η^{-n} . On top of it, the calculation has to be repeated for a number of different realizations of $|\Phi\rangle$ for random averaging to reduce the fluctuation arising from the use of random vectors. The scale of such computation can easily overwhelm the capacity of any computing facility in existence.

However, the computational load can be greatly reduced by inserting the completeness relation of the random phase vector¹⁾

$$\langle |\Phi\rangle \langle \Phi| \rangle_{\Phi} = I \quad (\text{identity operator}) \quad (5)$$

in the matrix element of Eq. (4) to decompose it into n factors.⁵⁾ The response function is then given by

$$\int_0^T dt_1 \int_0^{t_1} dt_2 \cdots \int_0^{t_{n-1}} dt_n e^{i(\omega_1 t_1 + \omega_2 t_2 + \cdots + \omega_n t_n)} \left\langle \langle \Phi_1 | \hat{O}_f e^{iHt_1/\hbar} \hat{O}_1 e^{-iHt_1/\hbar} | \Phi_2 \rangle \times \langle \Phi_2 | e^{iHt_2/\hbar} \hat{O}_2 e^{-iHt_2/\hbar} | \Phi_3 \rangle \cdots \times \langle \Phi_{n-1} | e^{iHt_{n-1}/\hbar} \hat{O}_{n-1} e^{-iHt_{n-1}/\hbar} | \Phi_n \rangle \times \langle \Phi_n | e^{iHt_n/\hbar} \hat{O}_n e^{-iHt_n/\hbar} \hat{O}_i | \Phi_1 \rangle \right\rangle_{\Phi_1, \dots, \Phi_n}, \quad (6)$$

where $|\Phi_i\rangle$'s are mutually independent random vectors. The computationally most costly process of integrating the Schrödinger equation is now used only to obtain n complex functions of a single time variable instead of a function with n time variables. Once the necessary complex-valued functions have been calculated and stored, the n -dimensional time integration may easily be done with a small computer. The computational load therefore scales only as η^{-1} with the energy resolution.

The effectiveness of the algorithm was first tested by calculating the two-photon absorption coefficient¹⁹⁾ of a fictitious system of electrons in a parabolic potential.⁵⁾ In the present scheme, the two-photon absorption coefficient of electrons exposed to monochromatic light of frequency ω is calculated according to the formula⁵⁾

$$\alpha^{(2)}(\omega) = \left\langle \left| \left(\frac{-e}{i\hbar} \right)^2 \int_0^T dt_1 \int_0^{t_1} dt_2 e^{-i(\omega-i\eta)(t_1+t_2)} \right. \right. \\ \times \left. \left\langle \Phi | \theta(H-E_F) e^{iHt_1/\hbar} \mathbf{r} e^{-iHt_1/\hbar} \theta(E_c-H) | \Phi' \right\rangle \right. \\ \times \left. \left. \left\langle \Phi' | e^{iHt_2/\hbar} \mathbf{r} e^{-iHt_2/\hbar} \theta(E_F-H) | \Phi \right\rangle \right|_{\Phi'}^2 \right\rangle_{\Phi} \quad (7)$$

The statistical averaging over the intermediate random vector $|\Phi'\rangle$ requires extra CPU time, so that the effectiveness of the method must be measured by the amount of CPU time required to attain certain specified statistical accuracy. The test revealed that the new method indeed holds advantage over the straightforward multi-dimensional integration, and that the relative advantage becomes greater for higher orders of nonlinearity and at higher energy resolution.⁵⁾ We then applied the method to the calculation of the two-photon absorption spectra of a realistic system of crystalline silicon.⁶⁾ The result is shown by the solid line in Fig. 4. The calculation is done for a cubic block of silicon crystal containing 4096 Si atoms, with the periodic boundary condition imposed on all faces. The total of 96^3 mesh points were taken in the cube. The empirical pseudopotential used for the Si atoms is the same as for other calculations. For comparison, the dotted line in Fig. 4 shows the theoretical result based on the band calculation using the non-local pseudopotential method.²⁰⁾ Peaks appear at similar energies in the two curves, giving them similar profiles. The agreement should be regarded as satisfactory in view of the different pseudopotentials used and the very different methods of calculation, and especially considering the level of agreement of either curve with the experimental result²¹⁾ shown by the circles in the figure.

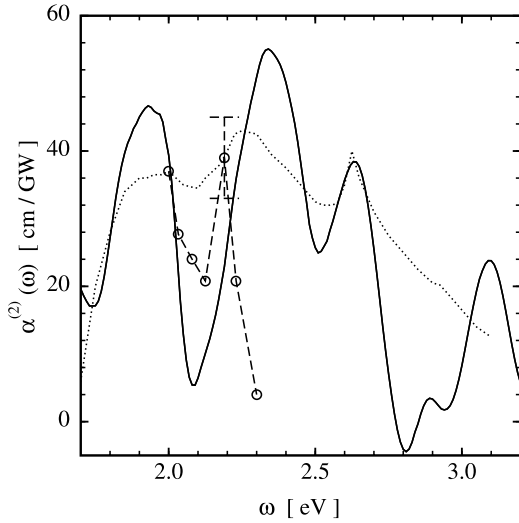


Fig. 4. The two-photon absorption spectra of bulk silicon. The solid line is the present result. The dotted line is the calculation of Ref. 20. The circles are the experimental data of Ref. 21.

Conclusion

The progress we have been making in the application of the real-time real-space higher-order finite-difference method has taken two directions. Since the method is formulated on a very general footing, one direction has been the application of the method to calculate dielectric function of various realistic complex systems. With the use of the empirical pseudopotential, there is no limit to the number of interesting systems to which the method can be applied to yield significant information. Such calculations should play an increasing role in the near future in the analysis of a wide range of systems from quantum microstructures to biological molecules. The other direction of progress has been the development of the method of computing non-linear response functions. For this purpose, however, the capacity of the present-day computers is still far from sufficient for a realistic calculation even with the use of the new fast algorithm. Progress will still be necessary both in the hardware and the algorithm before a meaningful comparison with experiment becomes feasible.

References

- 1) T. Iitaka, S. Nomura, H. Hirayama, X. Zhao, Y. Aoyagi, and T. Sugano: Phys. Rev. E **56**, 1222 (1997).
- 2) S. Nomura, T. Iitaka, X. Zhao, T. Sugano, and Y. Aoyagi: Phys. Rev. B **56**, 4348 (1997).
- 3) S. Nomura, T. Iitaka, X. Zhao, T. Sugano, and Y. Aoyagi: Phys. Rev. B **59**, 10309 (1999).
- 4) Y. Kurokawa, S. Nomura, T. Takemori, and Y. Aoyagi: submitted to Prog. Theor. Phys.
- 5) Y. Kurokawa, S. Nomura, T. Takemori, and Y. Aoyagi: Phys. Rev. E **59**, 3694 (1999).
- 6) Y. Kurokawa, S. Nomura, T. Takemori, and Y. Aoyagi: submitted to Prog. Theor. Phys.
- 7) R. N. Silver, H. Roeder, A. H. Voter, and J. D. Kress: J. Comput. Phys. **124**, 115 (1996).
- 8) O. F. Sankey, D. A. Drabold, and A. Gibson: Phys. Rev. B **50**, 1376 (1994).
- 9) A. L. Efros and A. L. Efros: Fiz. Tekh. Poluprovodn. **16**, 1209 (1982) [Sov. Phys. Semicond. **16**, 772 (1982)].
- 10) T. Takagahara and K. Takeda: Phys. Rev. B **46**, 15578 (1992).
- 11) S. Y. Ren and J. D. Dow: Phys. Rev. B **45**, 6492 (1992); J. P. Proot, C. Delerue, and G. Allan: Appl. Phys. Lett. **61**, 1948 (1992).
- 12) B. Delley and E. F. Steigmeier: Phys. Rev. B **47**, 1397 (1993).
- 13) L. W. Wang and A. Zunger: J. Chem. Phys. **100**, 2394 (1994).
- 14) S. Ögüt, J. R. Chelikowky, and S. G. Louie: Phys. Rev. Lett. **79**, 1770 (1997).
- 15) F. Huaxiang, Y. Ling, and X. Xide: Phys. Rev. B **48**, 10978 (1993); L. W. Wang: Phys. Rev. B **49**, 10154 (1994); K. Leung and K. B. Whaley: Phys. Rev. B **56**, 7455 (1997).
- 16) S. Nomura, X. Zhao, Y. Aoyagi, and T. Sugano: Phys. Rev. B **54**, 13974 (1996).
- 17) N. Matsumoto: Jpn. J. Appl. Phys. **37**, 5425 (1998).
- 18) D. C. Allan and J. D. Joannopoulos: Phys. Rev. Lett. **44**, 43 (1980); H. Teramae and K. Takeda: J. Am. Chem. Soc. **111**, 1281 (1989).
- 19) C. Cohen-Tannoudji, J. Dupont-Roc, and G. Grynberg: *Photons and Atoms*, (Wiley-Interscience, New York, 1997).
- 20) M. Murayama and T. Nakayama: Phys. Rev. B **52**, 4986 (1995).
- 21) D. C. Hutchings and E. W. Van Stryland: J. Opt. Soc. Am. B **9**, 2065 (1992).